Creep Buckling of Plates: Experiments on Aluminum Alloy at 500°F

RALPH PAPIRNO* AND GEORGE GERARD†
Allied Research Associates Inc., Concord, Mass.

Creep buckling and crippling experiments on long, simply supported plates of aluminum alloy 2024-0 at 500°F under axial compression were performed using a square tube configuration. An earlier exploratory program indicated that the conventional V-groove arrangement was unsatisfactory for use with this material at elevated temperatures. Short-time buckling and crippling experiments also were performed using the same experimental arrangement. An available constant strain-rate creep buckling theory for plates showed excellent correlation with the results of experiments on perfect plates. On less perfect experimental plates, where an arbitrary lateral deflection criterion of buckling was used, there were small discrepancies between short-time theory and short-time experiments, and similar discrepancies also were observed in the creep buckling data. However, when the effects of the discrepancies were suppressed by a normalization procedure based upon short time buckling, there was good correlation between the normalized constant strain-rate creep buckling theory and the normalized test data. In addition, a simplified approach for predicting creep crippling times showed good correlation with plate failure time data.

Nomenclature

E = modulus of elasticity, psi
E_t = tangent modulus, psi
E_s = secant modulus, psi
b = plate width, in.
h = plate thickness, in.
k = plate buckling coefficient
w = lateral deflection, in.
z = coordinate, in.
ϵ = strain, μ in./in.
$\dot{\epsilon}$ = strain rate, μ in./in./min
ϵ_{cr} = critical strain, μ in./in.
η = plasticity reduction factor
$\eta_{\dot{\epsilon}}$ = plasticity reduction factor, constant strain rate properties
ν = Poisson's ratio
ν_e = Poisson's ratio, elastic value
σ = stress, psi
σ_a = applied stress, psi
σ_{cr} = critical stress, psi
σ_{cy} = compression yield stress, psi
$\bar{\sigma}_f$ = crippling stress, psi

Subscript

0 = short-time conditions

1. Introduction

THERE are two distinct types of compressive instability phenomena associated with compression elements undergoing creep at constant load. Creep buckling is associated with the initial appearance of lateral deflections in the element; for such an element loaded to a stress level below its short-time critical stress, these deflections will occur some time after the creep load is applied. The time at which the lateral deflections occur is taken as the creep buckling time. If the element is of a type that can continue to support load after buckling, compressive creep continues, accompanied by further lateral deflection. Then, quite suddenly, the rate of change of lateral deflections increases, and in a very short time the element fails. The time of failure is taken as the creep crippling time.

Received January 2, 1963; revision received July 8, 1963. The research reported herein was sponsored by the U. S. Air Force under Contract AF 33(657)-8233 with New York University.

* Chief, Enviromechanical Sciences. Member AIAA.
† Vice President, Research and Engineering. Associate Fellow Member AIAA.

The primary objective of the experimental investigation reported herein was to obtain creep buckling times for long, simply supported plates and to use these experimental data to evaluate available theory.[1] A secondary objective was to obtain plate creep crippling times to assess the predictive value of a creep crippling analysis that is described in this paper. There have been only a limited number of flat-plate creep buckling experiments reported,[2–4] and in these experiments there was no distinction made between creep buckling and creep crippling.

The plate creep buckling theory described in Ref. 1 is pertinent to perfect plates and was an outgrowth of an earlier analysis of the creep buckling of perfect columns given in Ref. 5. The theory indicates that creep buckling solutions are analogous directly to short-time plastic buckling solutions with the material parameters derived from constant strain rate stress-strain curves. The latter are in turn constructed, using a graphical process from the compression creep curves of the material. Semiempirical approaches to this problem have been suggested in Refs. 2, 11, and 12.

Admittedly, it is not possible to manufacture and to test a perfect plate, i.e., one with no initial imperfections. However, it is possible to minimize initial imperfections by exercising great care in the manufacturing of the specimens and by taking pains to assure optimum experimental conditions when the tests are conducted. There is experimental evidence to indicate that theories based upon "perfect" structural elements can be correlated with data from "imperfect" elements provided that the imperfections are small.[5]

2. Experimental Boundary Conditions

A problem more serious in stability experiments than initial imperfections is simulating the mathematically assumed boundary conditions. In a plate, the boundary conditions along all four of the edges may be significant. However, in experiments on long plates loaded along the two short edges, the boundary conditions along the loaded edges are not of major significane. A small correction can be made to the buckling coefficient to take into account the actual elastic restraint at the loaded edges.

The experimenter has a choice for the unloaded plate edges of using either clamped or simply supported edges, since theoretical values of the buckling coefficient exist for each condition. Simulating clamped boundary conditions on the unloaded edges of a specimen plate and loading such a con-

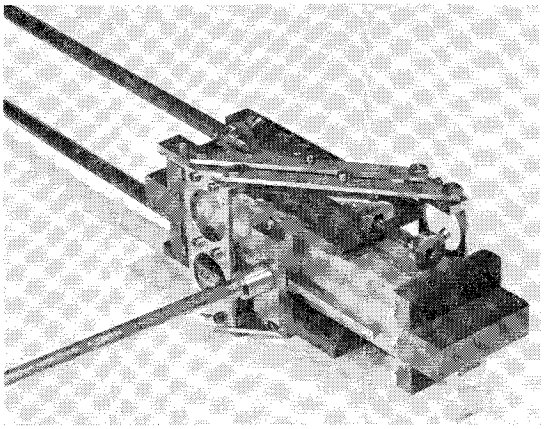

Fig. 1 Square tube plate specimen installed in instrumentation-loading jig.

figuration present formidable difficulties in the laboratory. Simulating simple-support boundary conditions on plates, although not in the category of a routine laboratory operation, presents fewer difficulties than simulating clamped edges.

Simply Supported Edges

Any configuration that simulates simple support must restrain lateral deflections of the long edges while allowing unrestricted rotation of the plate edges. In addition, it must not introduce significant in-plane forces into the plate, and it must offer little restraint to longitudinal compression of the plate. The ideal support jig would simulate the mathematically imposed boundary conditions as well as the other criteria while allowing plate growth due to thermal expansion and Poisson effects as well as in-plane edge displacements due to buckling.

A support jig was constructed with the V-groove-knife edge configuration. A series of experiments, the results of which are described in detail in Ref. 6, indicated that, although this arrangement was satisfactory for room temperature experiments on elastic plates, significant frictional effects developed at the 500°F test temperature in both short-time buckling and creep buckling experiments. These anomalous effects were detected by comparing autographically recorded end-shortening data from the buckling experiments with the appropriate compressive short-time stress-strain data and compressive creep data obtained from independent tests on material property specimens.

In the experiments reported in Refs. 2–4, a similar V-groove arrangement had been employed to simulate simple support. The possible frictional effects at elevated temperatures with this configuration make the reported data somewhat suspect.

Square Tube Configuration

It was clear that frictional effects had to be eliminated in the experiments if the correlation of test data with creep buckling theory was to be meaningful. An experimental configuration in which the mathematical boundary conditions for simple support can be simulated and in which frictional effects are absent is the square tube. As is well known, this configuration of four orthogonal flat plates does simulate simple support since, after buckling but prior to failure, the four unsupported edges remain straight ($w = 0$) and the corner angle remains a right angle ($\partial^2 w/\partial z^2 = 0$). In the past, difficulties in obtaining such tubular material in aircraft structural alloys or difficulties in fabricating this configuration from solid stock have limited its use in stability studies of flat plates. However, in view of the serious limitations of jigs in simulating the boundary conditions without introducing serious frictional effects into the test, it appeared that any extra efforts that would be required to fabricate square tube specimens would be clearly justified.

Aluminum alloy 2024 had been used previously, and, since it exhibited low scatter of properties at elevated temperatures, it was decided to continue with this material. Although it was not possible to obtain extruded square tubes in the 2024 aluminum alloy, extruded channel sections in this alloy were available. These were welded together to form the desired configuration using strips of the same alloy as the filler material.

3. Experimental Program

Plate Specimens

Extruded aluminum alloy 2024-T3 channel was received with the following cross-section dimensions: thickness $\frac{1}{8}$ in., base width 1 in., leg height $\frac{5}{8}$ in. In order to fabricate plates with a thickness ratio of approximately 25, the thickness was uniformly reduced to 0.040 in. by machining the inner surfaces of the channel. This procedure maintained the 1-in. base width. The leg height was reduced to $\frac{1}{2}$ in., and the free edges were bevelled externally to receive the filler material. Pairs of prepared channel sections were welded together to form square tubes using strips of the same aluminum alloy 2024-T3 as filler material. Excess filler material was machined away, and the square tube sections were cut into $4\frac{1}{8}$-in. lengths with the ends held parallel within ± 0.0005 in. The specimens then were annealed to the zero condition by the following heat treatment: 775°F 2 hr; cool to 500°F at 40°F/hr; furnace cool.

Material Property Specimens

Welded square tube specimens with the full $\frac{1}{8}$-in. wall thickness and 3-in. long were fabricated in the same fashion as the specimens. These were annealed simultaneously with the plate specimens, thus assuring that all specimen material would undergo exactly the same heat treatment.

Instrumentation for Lateral Deflection and End Shortening

Measurements of both lateral deflection and end shortening are desirable in buckling and crippling experiments. Buckling and crippling can be determined from the lateral deflection data, whereas the end shortening can be compared with the analogous short-time or creep strain data. In this connection, during short-time tests the stress-end shortening record should be comparable with the stress-strain curve for the test material until appreciable lateral deflections of the plate develop; in a similar fashion, during creep tests the end shortening-time record should be comparable with the creep strain-time curve for the material. Deviations between the analogous data when lateral deflections are small are indicative of anomalous effects in the experiment. It was just such deviations that led us to abandon the V-groove-knife edge configuration for simulating simple support.

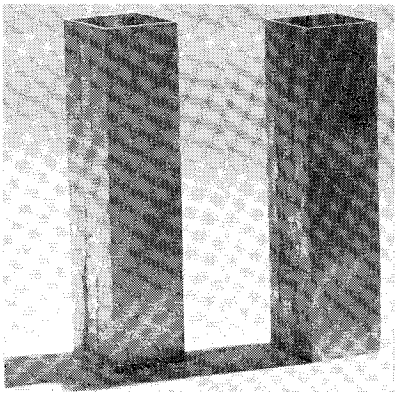

Fig. 2 Untested and crippled square tube plate specimens.

The lateral deflection instrumentation was designed to measure out-of-plane motions of either of the two opposite unwelded plates in the four-plate square tube configuration. A parallelogram linkage was arranged so that it would be displaced by the buckle of maximum amplitude wherever it occurred. Motions of the linkage with respect to an instrumentation mounting jig, fixed to the stationary ram of the testing machine, were transferred out of the furnace through a radial hole by concentric tube transfer elements to a differential capacitor sensor. The lateral deflection instrumentation and its supporting jig are shown in Fig. 1. It should be noted that no part of the supporting jig makes contact with the lateral surfaces of the specimen. The output of the differential capacitor was recorded. End-shortening measurements were made over a $3\frac{5}{8}$-in. gage length with gage points located $\frac{1}{4}$ in. from the specimen ends on two opposite sides of the configuration. The deflections were transferred out of the furnace by concentric tube strain transfer elements to separate differential capacitors. The separate measurements were averaged electrically and then recorded.

In the photograph of the installed specimen and instrumentation shown in Fig. 1 is a bearing block that is used to transmit the load from the movable ram of the testing machine to the specimen. A second bearing block for the stationary ram is integral with the instrumentation jig. Procedures, loading equipment, and autographic recording instrumentation are described in detail in Refs. 6–8.

All experiments were performed at 500°F with at least two specimens at each condition including short-time buckling and short-time crippling and creep buckling and creep crippling at 8400, 7840, 7280, and 6720 psi applied stress. Crippling times ranged from several minutes to several hours over the range of applied stresses. Crippling was evidenced by the simultaneous rapid increase of end shortening and lateral deflection that occurred, as will be shown subsequently, when the lateral deflection reached approximately 60% of the thickness.

A crippled specimen, together with an untested specimen, is shown in Fig. 2. It is evident that a number of buckle waveforms are present with one such waveform of slightly greater amplitude than the others. A careful examination of all tested plate specimens revealed that the maximum amplitude waveform did not occur in the same area in each specimen. This was an indication of lack of bias in the test procedure to favor a particular failure location.

Compressive Properties Tests at 500°F

Using the same procedures, loading apparatus, and autographic recording instrumentation as had been used in the plate experiments, both short-time and creep properties in compression were obtained using $\frac{1}{8}$-in.-thick wall, welded square tube specimens. Short-time tests and compressive creep tests were performed in duplicate at stress levels pertinent to those of the plate tests. Care was taken during the experiments to maintain a strain rate during loading of approximately 0.04 in./in./min, the value that had been used in the short-time and creep plate buckling experiments. The scatter of the strain values both for the short-time tests and the creep tests was found to be quite small.

4. Experimental Results

Properties of the Test Material at 500°F

The average short-time compression stress strain curve of the aluminum alloy 2024-0 test material at 500°F is shown in Fig. 3. Average compression creep curves of the specimen material are shown in Fig. 4.

The most probable value of the compression modulus of elasticity at 500°F under the strain rate conditions of the test as determined from the short-time tests and from the recorded stress strain curve during loading prior to creep tests was 8.0×10^6 psi.

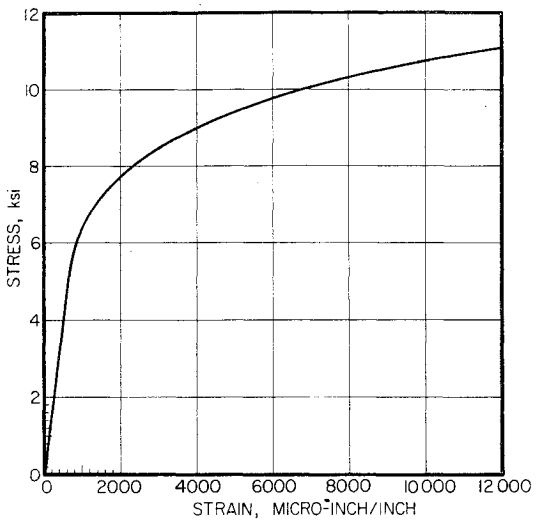

Fig. 3 Average short-time compression stress-strain curve of aluminum alloy 2024-0 at 500°F.

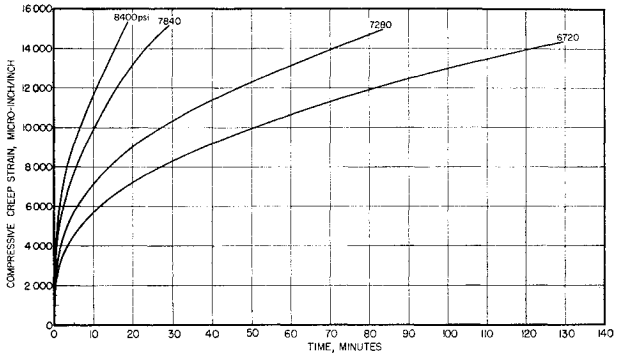

Fig. 4 Compression creep curves of aluminum alloy 2024-0 for various applied stress levels at 500°F.

End-Shortening and Lateral Deflection Data

End-shortening and lateral deflection data as a function of stress level from short-time buckling tests at 500°F are shown in Fig. 5. Also shown in the figure is the average short-time compressive stress strain curve. End-shortening and lateral deflection data as a function of time are shown in Figs. 6–9 for the following applied stress levels: 8400, 7840, 7280, and 6720 psi. In one experiment at 8400 psi, there was instrumental failure in the end-shortening recording system; hence the data are not given. Also shown in the figures are the appropriate creep curves for comparison with the end-shortening data.

In computing the value of the plate width-to-thickness ratio, it has been shown in Ref. 9 that the inside width of the square tube is the pertinent measurement to be used. The appropriate value for the width-to-thickness ratio for the specimens used in this investigation was $b/h = 23.0$.

Discussion of Experimental Results

The end-shortening curve closely follows the pertinent stress-strain or creep curve in most experiments until significant lateral deflections occur. This is an indication that the instrumentation and its supporting jig introduce little restraint to the square tube plate specimens. It is interesting to note that the first appearance of lateral deflections appears to have little influence on the end-shortening curve; hence the latter is an insensitive indication of plate buckling. Plate crippling, however, is accompanied by a large increase of end shortening.

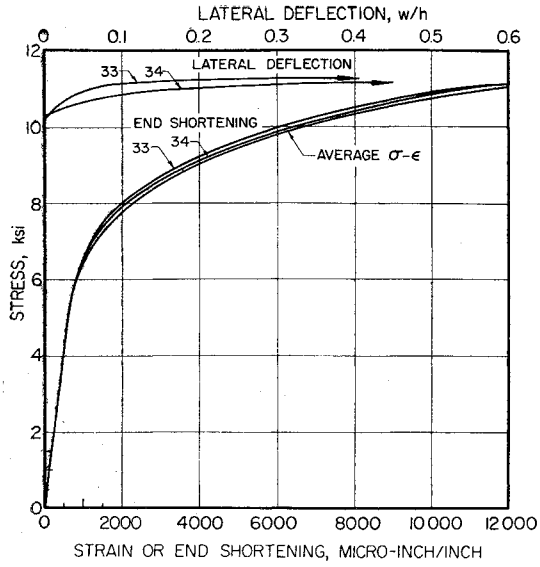

Fig. 5 End-shortening and lateral deflection data as a function of stress level for short-time buckling and crippling experiments on simply supported, long plates of aluminum alloy 2024-0 at 500°F with $b/h = 23$.

Since it is difficult experimentally to fabricate and test a perfect plate specimen, the choice of where buckling first occurs in terms of lateral deflection is somewhat arbitrary. In three experiments, however, the specimens were sufficiently "perfect" that lateral deflections occurred quite suddenly with a sharp break in the lateral deflection curve. These were the two short-time experiments and one creep buckling experiment at 7280 psi (specimen no. 23).

Accuracy of the Data

The loading equipment and recording instrumentation used in this study were the same as had been reported previously, and the statement on experimental accuracy given in Ref. 7 as applied to equipment and instrumentation would apply to the current experiments. Accuracy of the various system components is summarized as follows. 1) maximum extensometer error, 1%; 2) maximum loading system error, 0.5%; and 3) maximum spatial and temporal temperature variation, 2°F.

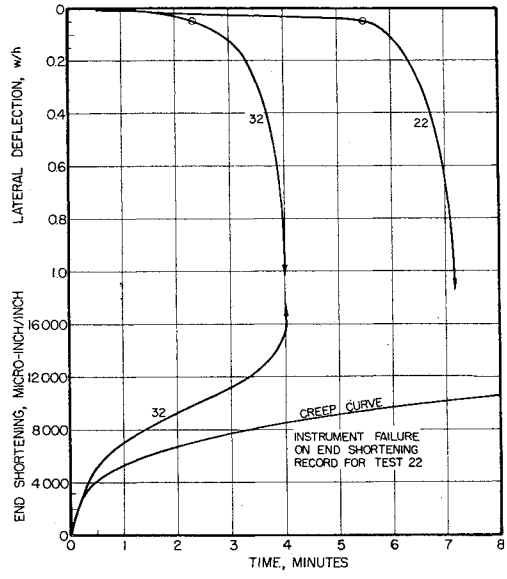

Fig. 6 End-shortening and lateral deflection data as a function of time for creep buckling and creep crippling experiments on simply supported, long plates of aluminum alloy 2024-0 at 500°F with $b/h = 23$; applied stress 8400 psi.

5. Correlation of Theory with Test Data

In the correlation of plate buckling theory with the test data, an inherent difficulty lies in establishing from the experimental data when buckling has occurred. In a short-time test, a plate can continue to support increasing loads after buckling, and sudden collapse does not occur until the crippling or failure load is reached. The latter can be considerably in excess of the buckling load. In creep experiments where a constant load is applied, the plate can continue to support the applied loading for relatively long times after buckling.

The use of a lateral deflection criterion for buckling of imperfect plates is far from ideal, since the degree of imperfection will influence the lateral deflection values. However, in the absence of other more rational criteria, it has been assumed arbitrarily that buckling has occurred when the lateral deflection reaches 5% of the plate thickness. In the few relatively "perfect" specimens, the buckling stress was chosen to coincide with a sharp break in the lateral deflection curve.

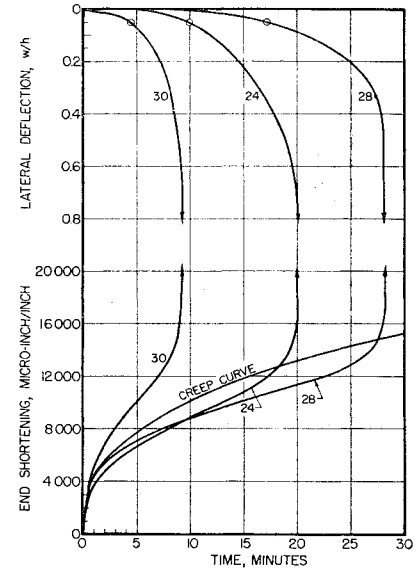

Fig. 7 End-shortening and lateral deflection data as a function of time for creep buckling and creep crippling experiments on simply supported, long plates of aluminum alloy 2024-0 at 500°F with $b/h = 23$; applied stress 7840 psi.

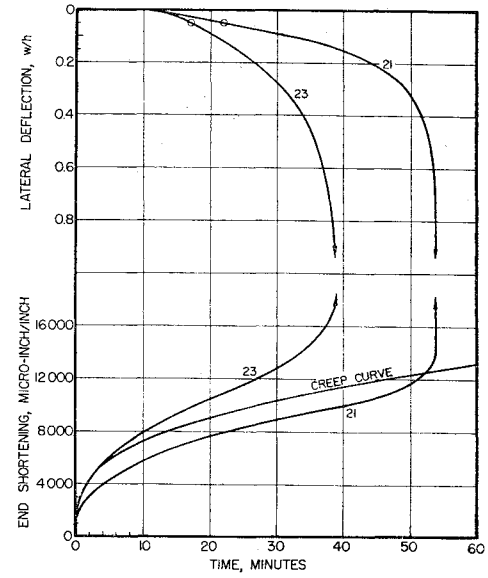

Fig. 8 End-shortening and lateral deflection data as a function of time for creep buckling and creep crippling experiments on simply supported, long plates of aluminum alloy 2024-0 at 500°F with $b/h = 23$; applied stress 7280 psi.

Short-Time Buckling

An appropriate solution for the short-time plastic buckling of long, simply supported plates has been given in Ref. 10 as

$$\sigma_{cr} = \frac{\pi^2 k \eta E}{12(1 - \nu_e^2)} \left(\frac{h}{b}\right)^2 \tag{1}$$

where

$$\eta = \frac{(1 - \nu_e^2)}{(1 - \nu^2)} \frac{E_s}{2E} \left[1 + \left(\frac{1}{4} + \frac{3}{4}\frac{E_t}{E_s}\right)^{1/2}\right] \tag{2}$$

and

$$\nu = 0.5 - 0.2\, E_s/E \tag{3}$$

For very long, simply supported plates, $k = 4$. However, in the experiments performed, the plates could be considered only moderately long with clamped conditions on the loaded edges, and for this case it is shown in Ref. 10 that $k = 4.15$.

From Eq. (1),

$$\frac{\sigma_{cr}}{\eta E} = \frac{\pi^2 k}{12(1 - \nu_e^2)} \left(\frac{h}{b}\right)^2 \tag{4}$$

Substituting the appropriate values of the constants in Eq. (4),

$$\sigma_{cr}/\eta E = 0.00709 \tag{5}$$

The left-hand side of Eq. (5) can be evaluated with the aids of Eqs. (2) and (3) and the short-time compression stress-strain curve to find the value of σ_{cr} which corresponds to Eq. (5). This value has been found to be $\sigma_{cr} = 10.0$ ksi.

Referring to Fig. 5, sharp breaks in the lateral deflection curves for the two specimens shown occur at 10.4 and 10.2 ksi. With this criterion of buckling, the errors are +4% and +2%, respectively. The probable cause of this discrepancy is believed to be the stiffening effect of small radii at the inner corners of this square tube. If the criterion for buckling is taken as a lateral deflection of 5% of the thickness, the discrepancy between theory and experiment is larger. A similar short-time discrepancy was observed for aluminum alloy columns at 500°F,[5] but this probably resulted from other causes.

Creep Buckling

In Ref. 1, it was shown that creep buckling solutions are analogous to plastic buckling solutions as given by Eq. (1), with the stipulation that the value of η becomes $\eta_{\dot{\epsilon}}$. The subscript $\dot{\epsilon}$ indicates that the appropriate material properties are derived from constant strain rate stress-strain curves, which in turn are derived by a graphical process from the compressive creep data. The process is described in detail in Ref. 1 but is summarized below.

The compressive creep curves given in Fig. 4 are differentiated graphically in order to obtain strain-strain rate data as shown in Fig. 10. Constant strain rate stress-strain curves from these data, shown in Fig. 11, are analyzed to obtain $\eta_{\dot{\epsilon}}$ and ν. On a plot of $\eta_{\dot{\epsilon}} E$ and σ a straight line corresponds to a particular value of the b/h ratio. Shown in Fig. 12 are such data with the straight line appropriate to $b/h = 23$ and $k = 4.15$, the conditions for the present set of experiments. Each intersection of this straight line with the curves of $\eta_{\dot{\epsilon}} E$ represents a unique set of conditions for creep buckling. In order to predict creep buckling times, one first finds the appropriate strain rate for buckling for the applied stress level from Fig. 12. Then, using an inverse process, one uses Figs. 10 and 4 to determine the theoretical creep buckling times.

Using the process just outlined, the theoretical curve shown as the solid curve in Fig. 13 was obtained. Shown in the figure by open circles are the experimental times for lateral

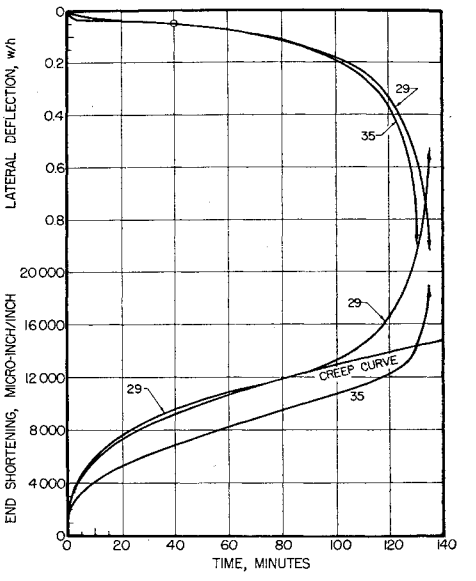

Fig. 9 End-shortening and lateral deflection data as a function of time for creep buckling and creep crippling experiments on simply supported, long plates of aluminum alloy 2024-0 at 500°F with $b/h = 23$; applied stress 6720 psi.

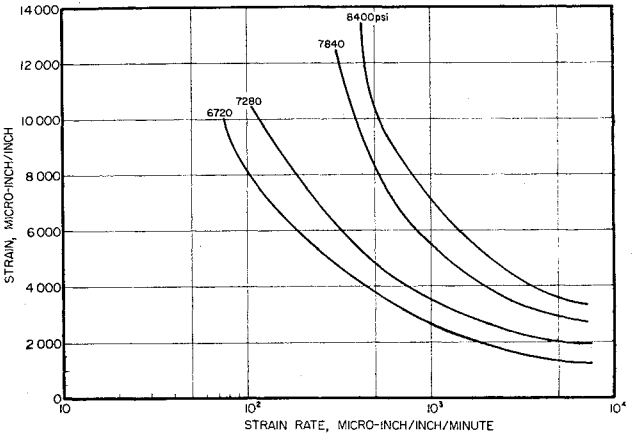

Fig. 10 Strain-strain rate data derived from Fig. 4.

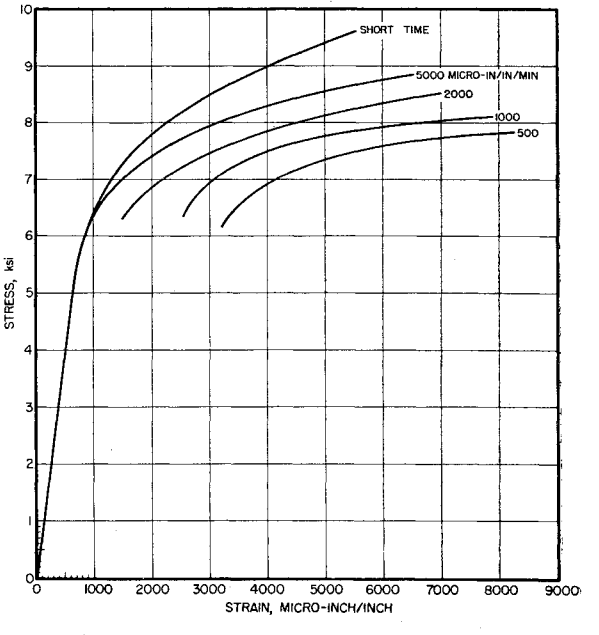

Fig. 11 Constant strain rate stress-strain data derived from Fig. 10.

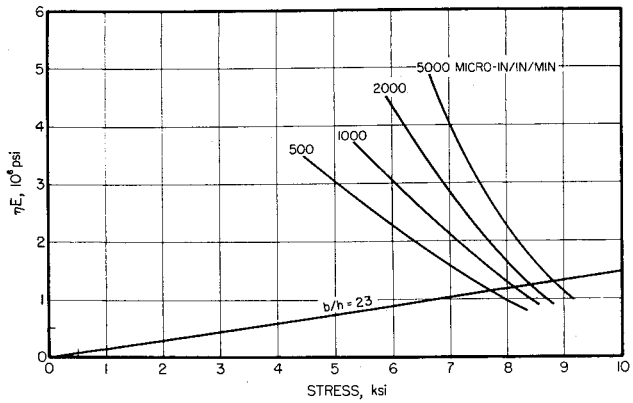

Fig. 12 Effective modulus-stress data for long, flat plates under axial compression as derived from Fig. 11.

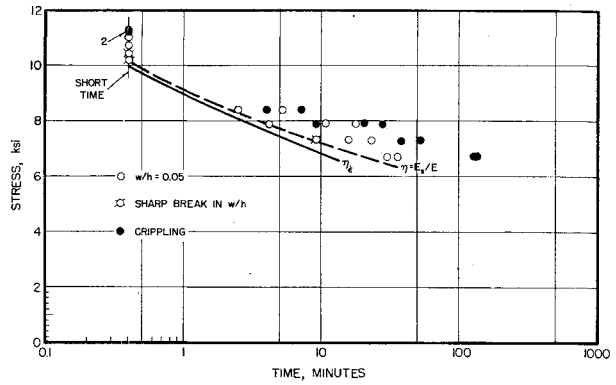

Fig. 13 Correlation of creep buckling theory and experiments for long, flat plates of aluminum alloy 2024-0 at 500°F under axial compression with $b/h = 23$.

deflections to reach 5% of the thickness, which have been designated arbitrarily as the buckling time. Also shown are the data for specimens that showed "sharp breaks" in the lateral deflection curves. The crippling or failure times have been indicated on Fig. 13 by closed circles. The data presented in the figure were obtained from Figs. 6–9. Short-time data from Fig. 5 are also given in Fig. 13. It is evident from the figure that the short-time discrepancy is reflected in the creep buckling results and that the theory more closely correlates with data from the more perfect specimens, i.e., those exhibiting sharp breaks in lateral deflection response.

An approach to creep crippling involves the use of the secant modulus as described in Ref. 11. If it is assumed that

$$\eta = \frac{(1 - \nu_e^2)}{(1 - \nu^2)} \frac{E_s}{E} \tag{6}$$

and Eq. (6) is substituted in Eq. (4),

$$\frac{\sigma_{cr}}{E_s} = \frac{\pi^2 k}{12(1 - \nu^2)} \left(\frac{h}{b}\right)^2 \tag{7}$$

but

$$E_s = \sigma/\epsilon \tag{8}$$

hence

$$\epsilon_{cr} = \frac{\pi^2 k}{12(1 - \nu^2)} \left(\frac{h}{b}\right)^2 \tag{9}$$

Equation (9) implies that the plate will cripple when the end-shortening strain reaches the critical value. The secant modulus results are shown as the broken curve in Fig. 13.

Normalized Stress Representation

A more rational correlation between the creep buckling data and the theory can be made if the discrepancies in the short-time results are suppressed, in view of the apparent dependence of creep buckling upon the short-time buckling behavior. This can be accomplished by normalizing theoretical creep buckling stresses to the appropriate short-time theoretical critical stresses and by normalizing the applied stresses to the appropriate short-time buckling stresses either the "sharp break" or the 5% thickness lateral deflection values for the experiments. Such a normalized representation is shown in Fig. 14. The normalized data are in substantial agreement with the normalized theory, indicating the procedure to be valid for the prediction of creep buckling times.

Although the constant strain rate theory was developed for the buckling of plates, it seemed interesting to examine its predictive value for plate crippling in normalized form. The theoretical creep buckling curve was normalized as before. The experimental applied stresses were normalized to the short-time crippling stresses. The results of this normalizing procedure are given in Fig. 15 as the solid curve. A similar normalizing procedure was applied to the secant modulus hypothetical approach, and the results are shown in Fig. 15 as the broken curve. As in the case of creep buckling, the data are in substantial agreement with both the constant strain rate approach and the secant modulus approach. In view of the facility with which the secant modulus hypothesis can be applied, it could be recommended for prediction of creep crippling times when used in normalized form.

6. Conclusions

The constant strain rate creep buckling theory as developed in Ref. 1 appears to provide a satisfactory lower bound to the creep buckling times observed for the plate tests reported herein. Similarly, the secant modulus approach to creep crippling provides a reasonable lower bound to the plate creep crippling data reported herein.

There are some discrepancies between short-time experimental plate buckling data and theory when a lateral deflection of 5% of the thickness is taken as the buckling criterion. These same discrepancies are preserved into the creep buckling region. On the other hand, when relatively perfect plate specimens are used in the experiments, correlation of theory with experiment is excellent both in the short time and creep cases.

If discrepancies due to the choice of the buckling criterion are suppressed by a normalization procedure, the normalized constant strain-rate plate creep buckling theory shows excellent correlation with plate creep buckling data. Since the results of the experimental program suggest a dependence of the creep instability behavior of plates on short-time behavior, short-time elevated temperature tests on plates

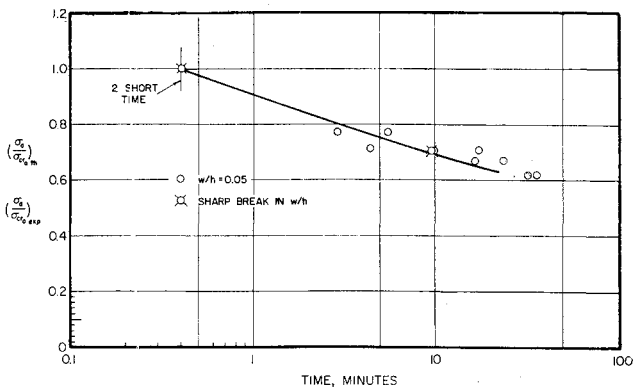

Fig. 14 Correlation of creep buckling theory with experimental creep buckling times for long, flat plates of aluminum alloy 2024-0 at 500°F under axial compression with $b/h = 23$, expressed in normalized form.

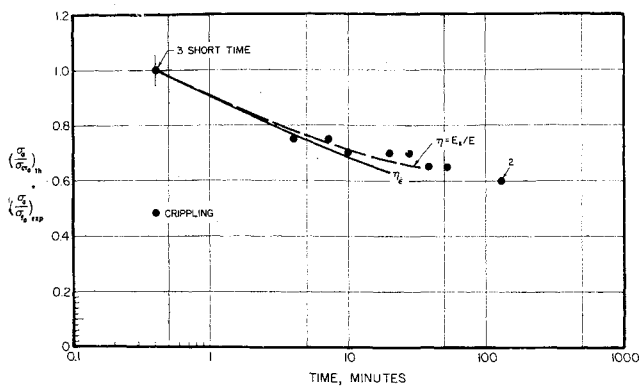

Fig. 15 Correlation of creep buckling theory and secant modulus approach with experimental creep crippling times for long, flat plates of aluminum alloy 2024-0 at 500°F under axial compression with $b/h = 23$, expressed in normalized form.

are necessary in order to establish a base point for the use of normalized theories of creep buckling and creep crippling.

References

[1] Gerard, G., "Theory of creep buckling of perfect plates and shells," J. Aerospace Sci. **29**, 1087–1090 (1962).

[2] Mathauser, E. E. and Deveikis, W. D., "Investigation of the compressive strength and creep lifetime of 2024-T3 aluminum alloy plates at elevated temperatures," NACA TN 3552 (January 1956).

[3] Deveikis, W. D., "Investigation of the compressive strength and creep of 7075-T6 aluminum-alloy plates at elevated temperatures," NACA TN 4111 (November 1957).

[4] Stein, B. A., "Compressive strength and creep of 17-7 PH stainless-steel plates at elevated temperatures," NACA TN 4296 (July 1958).

[5] Gerard, G. and Papirno, R., "Classical columns and creep," J. Aerospace Sci. **29**, 680–688 (1962).

[6] Gerard, G. and Papirno, R., "Correlation of plate creep buckling theory with experiments on long plates of aluminum alloy 2024-0 at 500°F," Aeronaut. Systems Div. TDR 62-865 (September 1962).

[7] Papirno, R. and Gerard, G., "Investigation of creep buckling of columns and plates, Part II: Creep buckling experiments with columns of Ti-7Al-4Mo titanium alloy," Wright Air Dev. Center TR 59-416 (July 1960).

[8] Papirno, R. and Gerard, G., "Compression testing of sheet materials at elevated temperatures," Am. Soc. Testing Materials Special Tech. Publ. 303, pp. 12–13 (1962).

[9] Becker, H., "Handbook of structural stability, Part II: Buckling of composite elements," NACA TN 3782 (July 1957).

[10] Gerard, G. and Becker, H., "Handbook of structural stability, Part I: Buckling of flat plates," NACA TN 3781 (July 1957).

[11] Gerard, G., "A creep buckling hypothesis," J. Aeronaut. Sci. **23**, 879–882 (1956).

[12] Bijlaard, P. P., Wong, R. E., Goldberg, M. A., and Dukes, W. H., "Strength analysis of high-speed-structures," Wright Air Dev. Center TR 55-305, Part 2, Sec. 7 (October 1955).

SEPTEMBER 1963 AIAA JOURNAL VOL. 1, NO. 9

Thermogalvanic Energy Conversion

R. Zito Jr.*
General Electric Company, Philadelphia, Pa.

Conversion from thermal energy to electrical energy has become an increasingly important area for investigation in recent years. A means for obtaining electrical power from thermal energy sources will be described here. The principle upon which this device is based is the change in chemical potential with temperature of a reversible cell. Some electrical and thermodynamic data are given for an elementary examination of device performance. Efficiencies and operating characteristics appear to be interesting for at least limited future application. However, greater understanding of the microscopic behavior is necessary in order to develop and improve materials handling, fabrication techniques, and cell construction.

Introduction

DEVICES that convert heat energy to electricity generally are referred to as thermoelectric generators. These devices almost invariably do not involve mechanical motion of any kind for their operation such as is necessitated in conventional rotating machinery. A well-known example of such static thermoelectric generators uses the Seebeck voltages produced at the junctions of dissimilar metal conductors and semiconductors when suitable temperature differentials are established between junctions.

Many aspects of the performance of thermoelectric devices must be considered in determining the extent of their utility. Among the more desirable and important parameters to be examined, the following may be listed: 1) high power-to-weight ratio (specific energy drain rate); 2) long operating and shelf life; 3) usable temperature range, both for high Carnot efficiency and in terms of conveniently available temperatures; 4) minimum complexity and moving parts; 5) ease of assembly and repair; 6) compatible materials combinations; 7) in cases of industrial or commercial application, low materials and fabrication costs; 8) capability of withstanding damage due to mechanical vibration, nuclear radiation, thermal shock, etc.; 9) high energy conversion efficiencies; and 10) convenient electrical output characteristics.

This paper will be concerned primarily with presenting the application of the thermogalvanic effect to the problem of thermoelectric power generation. This relatively unexplored approach, also referred to as ionic-thermoelectric conversion, appears promising. However, electrical conduction processes and thermoelectric phenomena in ionically conducting media such as ionic crystals have not received nearly the attention that pure metals and semiconducting materials have.

Received December 26, 1962; revision received July 12, 1963.

* Consulting Physicist, Space Technology Center, Missile and Space Division.